

PERSPECTIVES OF NUCLEAR PHYSICS

AMAND FAESSLER

*University of Tuebingen
Institute for Theoretical Physics
D-72076 Tuebingen, Germany*

The organizers of this meeting have asked me to present perspectives of nuclear physics. This means to identify the areas where nuclear physics will be expanding in the next future. In six chapters a short overview of these areas will be given, where I expect that nuclear physics will develop quite fast:

- (1) Quantum Chromodynamics and effective field theories in the confinement region.
- (2) Nuclear structure at the limits.
- (3) High energy heavy ion collisions.
- (4) Nuclear astrophysics.
- (5) Neutrino physics.
- (6) Test of physics beyond the standard model by rare processes.

After a survey over these six points I will pick out a few topics where I will go more in details. There is no time to give for all six points detailed examples. I shall discuss the following examples of the six topics mentioned above:

- (1) The perturbative chiral quark model and the nucleon Σ -term.
- (2) VAMPIR (Variation After Mean field Projection In Realistic model spaces and with realistic forces) as an example of the nuclear structure renaissance.
- (3) Measurement of important astrophysical nuclear reactions in the Gamow peak.
- (4) The solar neutrino problem.

As examples for testing new physics beyond the standard model by rare processes I had prepared to speak about the measurement of the electric neutron dipole moment and of the neutrinoless double beta decay. But the time is limited and so I have to skip these points, although they are extremely interesting.

1. The view from the top

1.1. *Quantum Chromodynamics and effective field theories in the confinement region*

We all are convinced that Quantum Chromodynamics (QCD) is the correct theory of the strong interaction. Thus all considerations about nuclear physics should be starting from QCD. But no-one will request that one is calculating the structure of ^{208}Pb using QCD. But one should calculate with lattice QCD the properties of the baryon resonances and the mesons. This is done presently with increasing success. The main problem in lattice QCD is to implement chiral symmetry, which is an important property of QCD. My friends working about QCD on the lattice tell me, that this problem has been solved within the last two years, at least in principle. But it is still numerically very difficult to reduce the masses of the quarks and the pion to reach the chiral limit. But one can for example take QCD lattice data and extrapolate it them with the help of chiral perturbation theory to the chiral limit.

Chiral Perturbation Theory (ChPT) can be proved¹ to be equivalent to QCD in a low energy limit. On the other side Weinberg and others^{2,3,4} did show that specific constituent quark Lagrangians are equivalent to an effective description of hadrons and their interaction. So one can expect that there exist effective field theoretical Lagrangians of quark models, which are equivalent in the low energy limit to QCD^{2,3,4,5}. But such an equivalence has not yet been proved.

The focus is presently on the structure of the nucleons (electromagnetic form factors) and on the strangeness in the nucleon (spin structure functions).

In the last years one has also learned to partition a process in a hard and soft part. For the hard part one can use perturbative QCD and for the soft part one can use models or experimental form factors. Such a process is shown with its lowest order diagram in figure 1.

One gets additional information by polarising the proton and the electron or the muon. Recently at HERMES and at COMPASS one discusses the situation were the proton is transversally polarized (transversity). Since the gluons like the photons have their spin in or against to the flight direction, they cannot contribute to the transversally polarized proton spin. Since the sea quarks and antiquarks are produced by the gluons, they are also not contributing to the proton spin, if the proton is polarized perpendicular to the beam axis. Thus the spin structure function for a proton

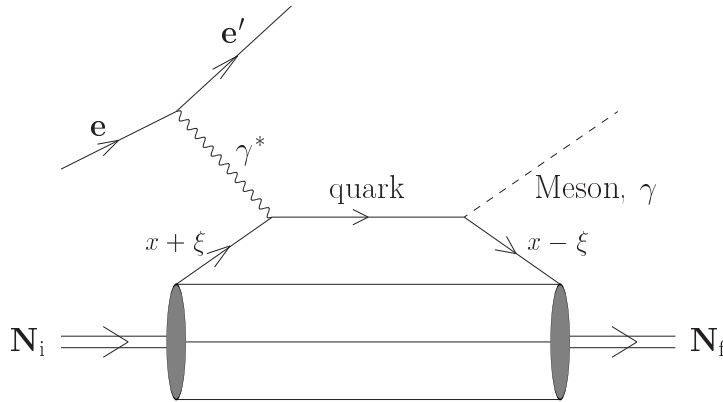


Figure 1. “Handbag” diagram for the electro production of a meson or a γ quant. This lowest order diagram partitions electro production of a meson or a gamma quant into a hard piece, involving one parton with the initial fractional momentum $x + \xi$ and the final fractional momentum $x - \xi$. The hard process of the electron scattering with the parton and the meson or the gamma production can be treated by QCD perturbation theory. The soft part of this reaction is parametrized by an off-forward form factor which not only depends on the momentum transfer Q^2 and on the momentum fraction of the interacting parton x , but on the momentum fraction of the parton in the initial state of the nucleon $x + \xi$ and on the momentum fraction of the parton in the final state of the nucleon $x - \xi$.

polarized in this way must be simpler than for a longitudinal polarized proton.

An open problem are hybrids and glueballs: hybrids are hadrons composed partially by quarks and partially by gluons. Exotic mesons would be composed of a quark and an antiquark and one or several gluons. They can have quantum numbers which are not allowed if they are built solely by a quark and an antiquark.

Glueballs are particles built only by gluons. The LEAR collaboration found a fifth neutral scalar “meson” with the quantum numbers 0^+ . For neutral scalar mesons only $a_0(1450)$, $K^{0*}(1430)$, $f_0(1370)$ and the $f_0(1710)$ should exist. Hence the $f_0(1500\text{MeV})$ could be a glueball. Indeed this state is only weakly decaying into two photons. A pure glueball cannot decay into two photons, since it does not contain any charged particles. But the weak decay into two photons already indicates that the $f_0(1500)$ can at the best be a mixture of a glueball with a quark - antiquark configuration. This

is also suggested by theoretical calculations^{6,7}.

In spite of the strong hints for the existence of exotic mesons and of glueballs they have not been detected out of any doubt.

1.2. Nuclear Structure

As mentioned already above, no-one will request that nuclei like ^{208}Pb are calculated starting from QCD. But we would like to understand the nucleon-nucleon interaction within the framework of QCD. Presently we have only QCD inspired models describing the nucleon-nucleon interaction^{8,9}.

From the bare nucleon-nucleon interaction one has to derive in a second step the effective nucleon-nucleon force for a given model space, in which the nuclear many-body problem is solved. This deduction of the effective nucleon-nucleon interaction from the bare nucleon-nucleon force has been studied since the 60ies. But the problem has not yet been solved quantitatively. A different question is then the derivation of the simple very successful nuclear models from the nucleon degrees of freedom and the effective interaction.

Presently we have a renaissance of experimental nuclear structure studies and the corresponding theoretical investigations. This renaissance is on one side due to the possibility of radioactive beams: accelerators like SPIRAL in Caen, RIKEN in Japan, the GSI in Darmstadt (existing and planned facilities), the Rare Ion Accelerator (RIA) discussed in the States and the smaller activities in Catania and Legnaro in Italy. On the other side this renaissance is due to new detector arrays like Euroball and the Gamma Sphere and plans of even more advanced gamma-ray detectors.

One aim is to study the shell structure of nuclei at the limits of stability for larger proton numbers Z and neutron numbers N . In the last years one found the celebrated neutron halos starting in ^{11}Li and proton skins, which are smaller than the neutron halos due to the high Coulomb barrier. One detected also new types of collective states: Dönau, Frauendorf and others^{10,11} predicted magnetic rotations in spherical nuclei. Hübel and Clark¹¹ found these states experimentally. The essence of these magnetic rotations are spherical nuclei, mostly with some proton holes just below a magic number and some neutron particles just above. Since particles and holes are repelling each other, the orbits of neutrons and protons try to have an overlap as small as possible (see figure 2).

Figure 3 shows such magnetic rotational bands with strong M1 tran-

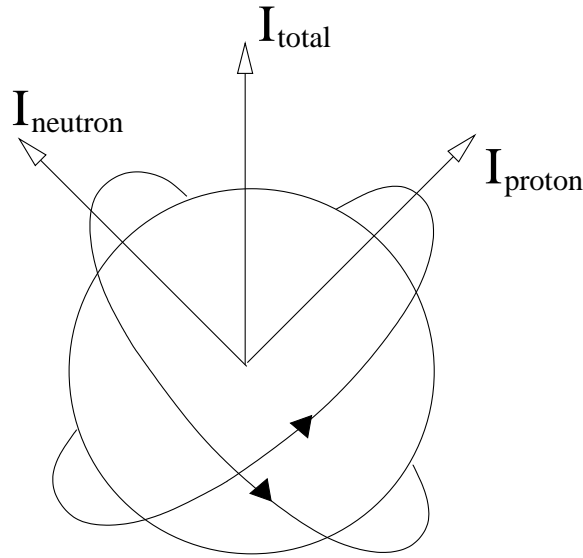


Figure 2. Magnetic rotational nucleus. The protons are normally hole states below a closed shell while the neutrons are particle states above a closed shell. Particles and holes are repelling each other, so that the orbits of proton holes and the neutron particles try to arrange with the least possible overlap. With increasing angular momentum the shear of the proton and the neutron angular momenta is closing and the energy band looks rotational. Since the shape of the nucleus is almost spherical, one has only very weak electric quadrupole transitions, but strong magnetic dipole M1 transitions. When the proton and the neutron angular momenta start to align, the M1 transitions are getting weaker, since the magnetic moment of the protons is along the proton angular momentum and the magnetic momentum of the neutrons is opposite to the angular momentum of the neutrons.

sitions measured in the $^{54}\text{Fe}(^{56}\text{Ni}, \alpha 4p)$ at a Ni kinetic energy of $E_{kin} = 243\text{MeV}$ by Jenkins et al. at Berkely ¹² in ^{102}Cd and ^{104}Cd .

Superdeformed nuclei with an axis ratio 2:1 have been already found in the 80ies. Hyperdeformed nuclei with an axis ratio 3:1 have been predicted by Strutinsky type calculations since a long time. But in spite of several announcements that such hyperdeformed nuclei have been found, such an axis ratio has been not yet clearly established.

The shell model technology made large progress over the last years ¹³. One is now able to diagonalized matrices of the many-body hamiltonian of around 100 millions times 100 millions. This allows to treat a many-body Hamiltonian exactly in the pf-shell. The Green's function Monte Carlo approach ¹⁴ allows to solve the nuclear many-body problem exactly

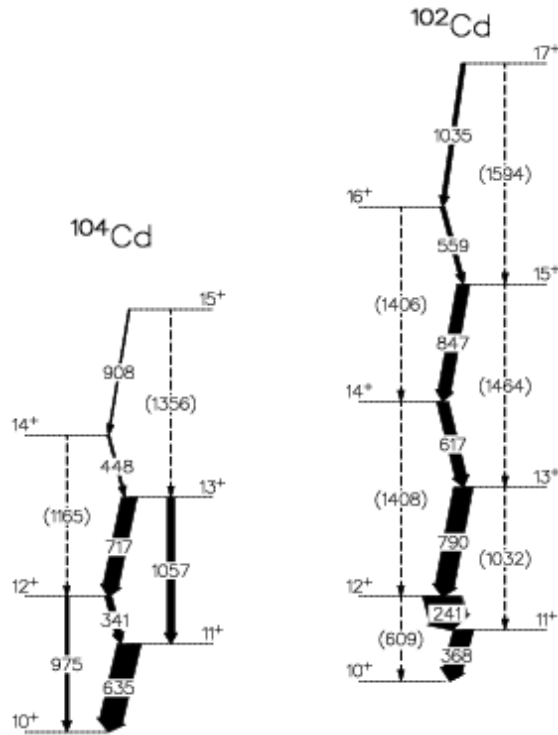


Figure 3. Magnetic rotational spectra of ^{104}Cd and ^{102}Cd . The protons form two holes in $g_{9/2}$ below the magic number 50 and the neutrons six particles in the $d_{5/2}$ and the $g_{7/2}$ shells. The width of the arrows between states with neighbouring angular momenta indicate the strength of the magnetic dipole M1 transitions, while $\Delta I = 2$ transitions are of E2 nature. One sees that with increasing angular momenta the magnetic dipole M1 transitions are reduced and that the electric quadrupole E2 transitions are always weaker than the M1 intensities. (Figure taken from D. G. Jenkins et al., arXiv: nucl-ex/0007004 v1.)

without any restriction for up to 8 or even 10 nucleons. A different approach is used in Tuebingen¹⁵ and Tokyo¹⁶. In the VAMPIR (Variation After Mean field Projection In Realistic model spaces and with realistic forces) and in the Monte Carlo shell model¹⁶ one is selecting the many-body basis states so carefully, that a few states are producing similar good results as a shell model diagonalization of several million configurations.

Relativistic nuclear structure approaches¹⁷ have the advantage, that they are able to describe the spin-orbit part of the self-consistent nucleon-nucleus potential quantitatively¹⁷.

1.3. High energy heavy ion collisions

One of the main aims of studying ultrarelativistic heavy ion collisions at CERN with the SPS, at Brookhaven with RHIC and in the future also with the ALICE detector at the LHC (Large Hadron Collider)/CERN is to study (and find) the phase transition from nuclear to quark matter.

The detection of the quark-gluon plasma has already been announced on February 10th, 2000 by CERN. For such a phase transition we have strong circumstantial evidence, but not a definite proof. The strong evidence is three fold:

- (i) The suppression of the J/ψ production in ultrarelativistic heavy ion collisions at SPS/CERN relative to the proton-proton reaction.
- (ii) An increase of the number of hadrons with strangeness content in ultrarelativistic heavy ion collisions relative to the proton-proton reaction at the same energy per nucleon.
- (iii) Hadrons are produced in ultrarelativistic heavy ion collisions in chemical equilibrium. This means that their relative abundance can be described by two parameters: a temperature and a chemical potential. Simulations which allow only the hadronic side, cannot reproduce well enough the hadron production in heavy ion collisions in chemical equilibrium. Thus one believes that the hadrons are produced during the condensation from the quark-gluon plasma into the hadronic phase in equilibrium characterized by the condensation temperature and the chemical potential for the baryon density.

At the ultrarelativistic heavy ion collisions at LHC (Large Hadron Collider at CERN) one should be able to study the melting of the vacuum. This means the restoration of chiral symmetry at high temperatures where one expects that the quark condensate $\langle \bar{q}q \rangle$, which has at zero temperature a finite expectation value, disappears $\langle \bar{q}q \rangle = 0$. The GSI plans to build a heavy ion collider with about 25 GeV per nucleon to study a possible phase transition from hadronic to quark matter at high baryonic density.

Figure 4 shows the temperature against the baryon chemical potential μ_B . The phase transition line expected from lattice QCD and the temperatures and chemical potentials determined from the multiplicity of hadrons produced in heavy ion collisions at different accelerators are displayed.

At RHIC one found a quite surprising result: Quarks are moving through a nucleus without losing too much energy (color transparency),

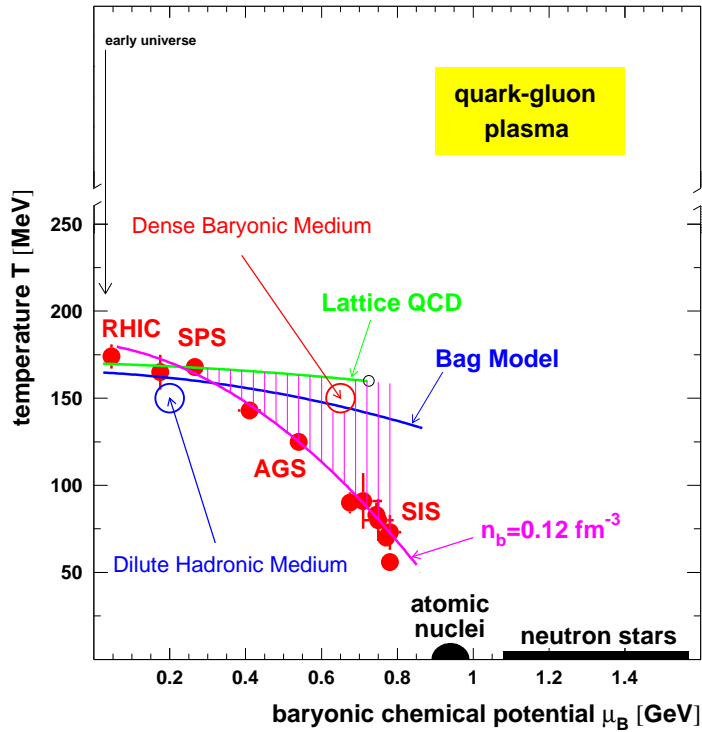


Figure 4. Phase diagram of the temperature against the baryon chemical potential. One line indicated “lattice QCD” shows the phase transition obtained in lattice QCD from nuclear to quark matter. The other lines with the dots and the bars show the temperatures and the chemical potentials determined in different heavy ion reactions and at different accelerators (RHIC, SPS, AGS and SIS) extracted from hadron multiplicities after heavy ion collisions. The baryon chemical potential μ_B in atomic nuclei is roughly given by the nucleon mass of 938 MeV. (Figure taken from P. Braun-Munzinger, J. Stachel, J. Phys. G 28, (2002) 1971 - 1976.)

while in a quark-gluon phase, due to open color a quark is frequently interacting and producing gluons.

Figure 5 shows the number of neutral pions produced in heavy ion collisions (mainly Pb on Pb at CERN and Au on Au at RHIC) relative to the number of neutral pions in proton-proton collisions scaled to the collisions of the indicated two heavy nuclei. A surprising result is, that this ratio behaves quite differently for the collisions at the SIS and at RHIC. The

value 1 would be obtained, if nothing new happens in heavy ion collisions compared to proton-proton reactions. That the number of neutral pions in Au on Au collisions is below unity at RHIC might indicate that the quark-gluon plasma is reached at RHIC. But it would also suggest that at CERN one still might have by large the color transparency situation with high energy jet. But the interpretation of these data is not obvious. But it is clear that something dramatically happens between the SIS and the RHIC energies.

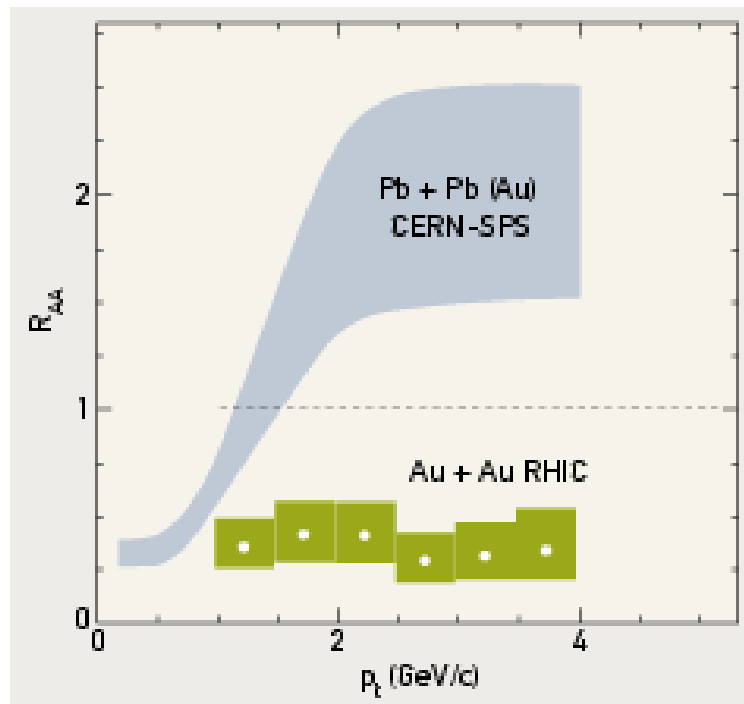


Figure 5. Number of neutral pions in heavy ion collisions compared to the number of neutral pions in the proton-proton reaction scaled to the heavy ion reaction as a function of the perpendicular momentum of the emitted particles. Without any new effects in heavy ion collisions this ratio should be unity. That this ratio behaves differently for the data from the SIS/CERN and for the data from RHIC/Brookhaven indicates that something dramatically happens between the SPS cm energy of 17 GeV per nucleon and for RHIC cm energy of up to 200 GeV per nucleon in the center of mass system.

An open question is also the nature of the phase transition from nuclear to quark matter: is it a first or second order phase transition or is there

a critical point where the phase transition on the right-hand side is of first order and on the left-hand side is smooth and of second order. A first order phase transition would indicate large fluctuations in the growth of the hadronic droplets in the big bang. This would immediately introduce large inhomogeneities of hadronic matter in our universe. Such large fluctuations have been seen by Boomerang and by Maxima in the cosmic background radiation.

1.4. *Nuclear astrophysics*

The measurements of Boomerang and Maxima of the cosmic background radiation show in their multipole decomposition of the fluctuations that the total energy density in our universe should be very close to the critical density, which produces a flat space. The heights of the second maximum indicates that hadronic matter is of the order of 5 % of the saturation density. Since dark matter is about 30 %, it leaves 65 % of the saturation density for vacuum energy or for a cosmological constant. This is in agreement with the relative abundance of the light elements produced in the big bang, which indicates also hadronic matter of the order of 5 %. The motion of the galaxies and the motion of stars in the halo of our galaxy suggest dark matter of about 30 % of the saturation density. Visible matter in the universe is below or of the order of 1 %. A large vacuum energy or a cosmological constant is also indicated by the observation of supernovae explosions at very far distances.

What is the nature of dark matter and of the vacuum energy or the cosmological constant? Is dark matter composed of weakly interactive massive particles (WIMP's) as suggested by the DAMA experiment in the Gran Sasso ¹⁸. Or can dark matter be explained trivially by a modification of Newton's law at small accelerations? ¹⁹.

To study the formation of elements in stars, one needs to know a large number of cross-sections at extremely small energies (see discussion below).

Medium heavy and extremely heavy nuclei are produced in the s-, p- and in the r-process.

In the s-process one needs a location where one produces neutron fluxes of about 10^8 neutrons per cm^2 and per second. In this case the beta decay (β^-) probability is faster than the (n, γ) reaction. Thus the s-process follows the stable nuclei. In the r-process one needs neutron fluxes which are about 14 orders of magnitude larger. The time for the fusion of a neutron to a nucleus in a (n, γ) reaction is much smaller than the time for the β^-

decay. One therefore forms nuclei with an extremely large neutron number up to the next magic shell, where the neutrons get unbound. There then they decay back to the stable nuclei in β^- processes.

The p-process happens in double stars with a white dwarf or a neutron star and a red giant. Hydrogen is flowing from the red giant to the white dwarf into an accretion disk and is exploding after enough hydrogen has been accreted on the surface of the white dwarf to ignite the fusion of hydrogen with the nuclei at the surface of the white dwarf. This produces very proton rich nuclei, which decay by β^+ reactions back to the stable nuclei.

An open problem are supernovae explosions. They are triggered after large stars of about 10 to 20 times solar masses have formed an inner Fe and Ni core. The collapse of the stars starts after one reaches the condition

$$m_e c^2 + \epsilon_F \geq (m_n - m_p) c^2 = 1.293 \text{ MeV}. \quad (1)$$

If the rest mass of the electron and its Fermi energy ϵ_F is getting larger than the mass difference between the neutron and the proton of 1.293 MeV the inverse beta decay sets in.



With the inverse beta decay the electrons are disappearing out of the star and the electron neutrinos can escape and so the Fermi pressure of the electrons is reduced and the star starts to collapse. This collapse goes on until the inner part of the Fe and Ni core has a density of about 10^{12} g/cm^3 . At this density the neutrinos of the reaction of the inverse beta decay (2) cannot any more escape and they trigger a shockwave which leads to the explosion of the star. But in all the simulations one does not have enough energy in the neutrinos to explode the star. This is mainly due to the fact that the inner core of Fe and Ni with the density larger than 10^{12} g/cm^3 is surrounded by a large sphere of Fe and Ni of lower density through which the shock has to travel. The energy which is needed to break up the Fe and Ni layer stalls the shock.

Recently Langanke suggested, that the inverse beta decay (2) leaves much more electrons in the center of a collapsing star, than expected up to now. Since the high density area, in which the electron neutrinos are trapped has a radius proportional to the remaining electron density squared, the shock wave has to travel through a much smaller layer of Ni and Fe nuclei. This could be perhaps one of the reasons why indeed supernovae are exploding in reality and not in simulations. But another reason could

be that all the calculations until now are either one or two dimensional. A three dimensional calculation would allow much smaller eddies and by that the situation of the exploding star would be quite different. Naturally there could also be missing some until now unknown piece of microphysics.

1.5. *Neutrino physics*

Neutrino physics is presently a very fast developing field. The development of neutrino physics was in recent years mainly fuelled by the solar neutrino problem. The solar neutrino puzzle can be solved assuming that the neutrinos are massive and that the mass eigenstates are different from the production or the weak or flavour eigenstates. All solar neutrino detectors, the Cl detector in the homestake mine (Nobel price 2002 to Ray Davies), the Ga detectors GALLEX and SAGE, the KAMIOKA, the Super-KAMIOKA (Nobel price 2002 to Masatoshi Koshiba) and also the SNO detectors indicate that neutrinos are missing. The same result was obtained from the atmospheric neutrinos, produced by cosmic radiations in the atmosphere. Muon neutrino produced at the opposite side of the earth are disappearing to a large amount until they reach the Super-KAMIOKA detector in Japan. The Sudbury neutrino observatory (SNO) in Canada could solve the problem by measuring at the same time the neutral and the charge current reactions of the neutrinos, using heavy water. The two measurements (where the charge current reactions were borrowed from Super-Kamiokande) allow to determine the total neutrino flux of electron, muon and tauon neutrinos. This total neutrino flux corresponds to the expected electron neutrino current from solar models.

The neutrino oscillations request a small extension of the standard model: neutrinos must have masses, which are different from each other. Since the oscillations depend only on the neutrino mixing matrix of the unitary transformation from the neutrino mass eigenstates to the flavour eigenstates and on the squares of the differences of the neutrino masses, one cannot determine an absolute mass scale. But (in the so-called natural hierarchy) the mass difference between the lowest and the second lowest neutrino masses must be of the order of 10^{-3} to 10^{-2} eV, while the mass difference between the second and the third neutrino is of the order of 10^{-1} to 1 eV.

1.6. *Test of new physics beyond the standard model*

The standard model of the electroweak (Glashow, Salam and Weinberg, 1968) and the strong interaction (Quantum Chromodynamics = QCD) is extremely successful. But it has also 16 free parameters (six quark masses, three mixing angles and one phase of the Cabibbo, Kobayashi and Maskawa unitary matrix, three coupling constants and the three masses of electrons, muons and tauons. These 16 parameters have to be supplemented by three neutrino masses, three mixing angles and one phase of the neutrino mixing matrix).

The standard model seems to be an effective field theory, which is exactly valid at energies far below the Grand Unification scale of the order of 10^{15} GeV. By embedding the standard model in a Grand Unified model or in supersymmetric or even superstring models reduces the number of parameters. In Grand Unified theories the electroweak and the strong interaction is described by one single force with one coupling constant.

Possible new physics from Grand Unification, supersymmetry (but probably not from superstrings) might be tested at ultrahigh energies at the LHC or perhaps also at TESLA/DESY. But several aspects of theories beyond the standard model can also be tested at low energies by looking to rare events.

Massive neutrinos with a unitary mixing between the mass and the flavour eigenstates allow for example the conversion of muons into electrons on nuclei. Figure 6 shows a possible diagram which contributes to this muon to electron conversion on nuclei, which is studied experimentally e. g. at the Paul-Scherrer-Institute (PSI).

Apart of the muon-electron conversion on nuclei, which tests only the hypothesis of massive neutrinos and their mixing, one can test Grand Unification in the neutrinoless double beta decay:

Figure 7 shows that the neutrinoless double beta decay is only possible if the neutrino and the antineutrino are identical particles, which means the neutrino must be a Majorana particle. This is predicted by most of the Grand Unified theories. In addition for left-handed weak interaction theories, one has a mismatch between the helicity of the emitted antineutrino and the absorbed neutrino. For massive neutrinos helicity is not a good quantum number and thus the double beta decay is possible in Grand Unified theories with massive Majorana neutrinos. Already now the lower limit of the lifetime for the neutrinoless double beta decay of the order of 10^{25} years for ^{76}Ge ²⁰ allows to restrict severely parameters of Grand Unified

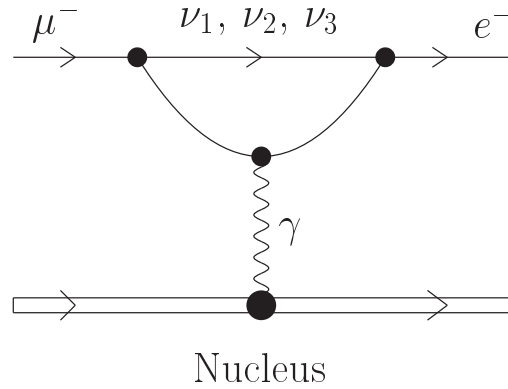


Figure 6. One diagram for the muon-electron conversion on nuclei which is allowed by intermediate massive neutrinos and the unitary mixing of the production eigenstates ν_e, ν_μ and ν_τ and the neutrino mass eigenstates ν_1, ν_2 and ν_3 .

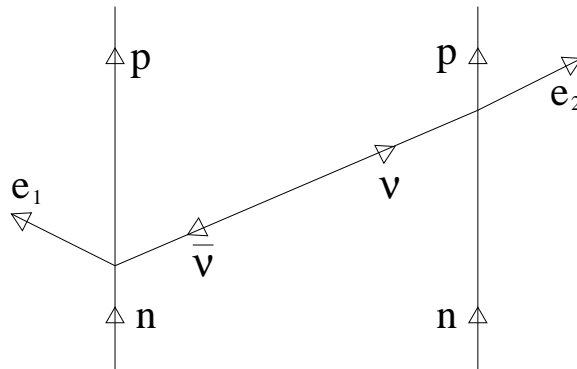


Figure 7. This figure shows the simplest diagram of the double neutrinoless beta decay where two neutrons in a nucleus are converted into two protons, which stay in the nucleus. Two electrons are emitted and can be detected. Presently it seems that the neutrinoless double beta decay has not been seen experimentally, although the Heidelberg group of Klapdor and collaborators claims, that they have seen the process.

theories and of the supersymmetric model.

Very interesting is also the electric dipole moment of the neutron. It has been studied experimentally at the ILL in Grenoble and at Gatchina

in St. Petersburg. The present value lies at

$$d_n \lesssim 10^{-26} e \cdot cm. \quad (3)$$

It is easy to see that an electric dipole moment requests violation of time reversal symmetry and of parity (see fig. 8).

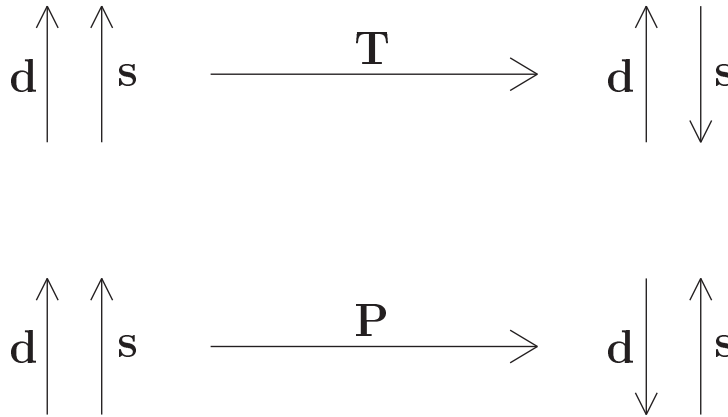


Figure 8. Electric dipole moment of the neutron. Since the spin of the neutron is the only specific direction the dipole moment has to be parallel or antiparallel to the spin. Time reversal does not change the direction of the dipole moment, but the direction of the spin and thus time reversal symmetry requests a zero electric dipole moment (see upper part of the figure). The parity operation does change the direction of the dipole moment, but not the direction of the spin. The lower part of the figure shows that conservation of parity requests a zero electric dipole moment of the neutron. The CPT theorem indicated that time reversal symmetry must be violated if CP is not a good symmetry. Violation of parity is well-known. Since time reversal and parity are violated, there must be at some level an electric dipole moment of the neutron. The present upper limit is given in equation 3 ($10^{-26} e \cdot cm$). The electroweak standard model predicts an electric dipole moment of the neutron of the order of $10^{-32} e \cdot cm$. But extensions of the standard model predict much larger electric dipole moments of the neutron. Improving the upper limit for the electric dipole moment of the neutron means to exclude some of these models which go beyond the standard model.

2. Examples from different fields

2.1. The perturbative chiral quark model ($P\chi QM$)

The Lagrangian of Quantum Chromodynamics (QCD) is invariant under the $SU(3)_L$ and $SU(3)_R$ flavour transformation for the first three quarks: u, d and s. If the current masses of this quarks are put equal to zero.

$$\mathcal{L}_{QCD} = \sum_f \bar{\Psi}_f (i\mathcal{D} - \hat{m}_f) \Psi_f - \frac{1}{4} F_{\mu\nu}^a F_a^{\mu\nu}$$

$$\text{with } \mathcal{D} = \gamma^\mu \left(\theta_\mu + \frac{i}{2} g \lambda_a A_\mu^a \right) \quad (4)$$

$$F_{\mu\nu}^a = \partial_\mu A_\nu^a - \partial_\nu A_\mu^a - g f_{abc} A_\mu^b A_\nu^c.$$

This means that the right-handed quarks (index R) stay always right-handed and left-handed quarks stay (index L) always left-handed in the chiral limit.

$$q_{L/R} = \frac{1}{2} (1 \mp \gamma^5) \begin{pmatrix} u \\ d \\ s \end{pmatrix}$$

$$m_f \bar{\Psi}_f \Psi_f = \hat{m}_f [\bar{\Psi}_{fL} \Psi_{fR} + \bar{\Psi}_{fR} \Psi_{fL}]. \quad (5)$$

The lower index f runs over the three flavours up u, down d and strange s. The indices a, b and c run over the three colors and f_{abc} is the structure constant of SU(3), and λ_a are the Gell-Mann color matrices. The second part of eq. (5) shows that the mass term with finite current masses of the quarks m_f violates chiral symmetry and scatters right-handed into left-handed and left-handed into right-handed quarks.

The perturbative chiral quark model^{21,22,23} uses like chiral perturbation theory the non-linear σ model to restore chiral symmetry even under the presence of a confining scalar $S(r)$ and perhaps also vector potential^{24,25}. The chiral perturbation theory¹ eliminates quarks and gluons and describes everything on the level of hadrons and the pseudoscalar Goldstone bosons. It has been shown that this approach is equivalent in a low energy limit to QCD as an effective field theory if the free parameters are adjusted accordingly. The perturbative chiral quark model (P χ QM) can be shown to be equivalent to a description on the hadron level including all hadrons^{2,3,4,5}, if one chooses form factors of the hadrons for the decomposition into quarks, which are Lorentz and Gauge invariant and fulfill the Ward identities. A proof, that the P χ QM is at low energies equivalent to QCD, does not exist.

If one expands the effective Lagrangian of the P χ QM up to second order in the pion field and restricts the expression to SU(2)-flavour, one obtains:

$$\mathcal{L}_{P\chi QM} = \mathcal{L}_0 + L_{int} + 0(\pi^3)$$

$$\begin{aligned}
\mathcal{L}_0 &= \bar{\Psi}_q \{i \not{\partial} - S(r) - \gamma^0 V(r)\} \Psi_q \\
&\quad - \frac{1}{2} \bar{\pi} \{ \partial_\mu \partial^\mu + m_\pi^2 \} \pi(x) \\
\mathcal{L}_{int} &= -\frac{1}{f_\pi} S(r) \bar{\Psi}_q i \gamma^5 (\vec{\tau} \cdot \vec{\pi}) \Psi_q \\
&\quad + \frac{1}{2f_\pi^2} S(r) \bar{\Psi}_q \vec{\pi} \cdot \vec{\pi} \Psi_q \\
\Psi_q &= \sum_\alpha b_\alpha u_\alpha(x) + \sum_\beta d_\beta^+ v_\beta(x).
\end{aligned} \tag{6}$$

In this expression we replaced the form factors for the decomposition of the nucleons into quarks by a scalar $S(r)$ and a vector $V(r)$ confining potential. This naturally violates Lorentz and Gauge invariance. But the model is presently improved by removing these potentials and having instead Lorentz and Gauge invariant form factors, which connect the hadrons with the quarks. The quark wave function ψ_q is calculated by solving the Dirac equation and one obtains bound state quark wave functions $u_\alpha(x)$ and the corresponding quark annihilation operator b_α . At the same time one obtains also the wave function for the antiquarks (v_β). But due to the presence of the vector potential $V(r)$, which changes sign from quarks to antiquarks, the model cannot be applied to calculate antiquark and thus also antinucleon wave functions. This difficulty does not exist if one introduces Lorentz and Gauge invariant form factors for the decomposition of the hadrons into quarks.

The first term of the interaction Lagrangian \mathcal{L}_{int} in eq. (6) is the usual pseudoscalar coupling of the pions to quarks. One can show by a unitary transformation that this term can be transformed into the pseudovector coupling. The two formulations are completely equivalent²⁶. The second interaction term is the so-called Seagull term, which is obtained by the expansion up to second order of the non-linear σ model. The original Lagrangian of the P χ QM fulfils the Gell-Mann Oaks Renner and the Gell-Mann Okubo relations.

$$\begin{aligned}
m_\pi^2 &= 2\hat{m} B ; m_K^2 = (\hat{m} + \hat{m}_s)B \\
m_\eta^2 &= \frac{2}{3}(\hat{m} + 2m_s)B \\
3m_\eta^2 + m_\pi^2 &= 4m_K^2 \\
\text{with : } B &\equiv -\langle 0 | \bar{u} u | 0 \rangle = m_\pi^2 / (2\hat{m}) \\
&= 1.4 [GeV]
\end{aligned} \tag{7}$$

$$\begin{aligned}\hat{m} &= \frac{1}{2} (\hat{m}_u + \hat{m}_d) = 7MeV \\ \hat{m}_s &= 175MeV.\end{aligned}$$

The scalar and vector confining potential $S(r)$ and $V(r)$ are parametrized by the solution of the Dirac equation in an oscillator potential by two parameters, which are fitted to the axial vector coupling constant $g_A = 1.25$ and to the mean squared radius of the quark content of the nucleon $\langle r_{charge}^2 \rangle = 0.6 \pm 0.1 [fm^2]$.

$$q_{1s}(\vec{r}) = N \exp\left[-\frac{r^2}{2R^2}\right] \left(\frac{1}{i\rho \frac{\vec{\sigma} \cdot \vec{r}}{R}} \right) \chi_s \chi_f \chi_G. \quad (8)$$

The two parameters fitted are R , which parametrizes the radius of the quark content of the nucleon and ρ which determines the importance of the two small relativistic components. ρ is adjusted to the axial coupling constant.

$$g_A = \frac{5}{3} \left[1 - \frac{2\rho^2}{1 + \frac{3}{2}\rho^2} \right] = 1.25. \quad (9)$$

Here I want to show the application of this model to the pion nucleon Σ -term, including $SU(3)$ flavour.

$$\begin{aligned}\sigma_N^\pi &\equiv \hat{m} \langle p | \bar{u} u + \bar{d} d | p \rangle \\ &= \hat{m} \frac{\partial m_N}{\partial \hat{m}} \\ \mathcal{H}_{\chi SB} &= \bar{q} \mathcal{M} q + \frac{B}{8} T_r \{ \Phi, \{ \Phi, \mathcal{M} \}_+ \}_+ \\ \mathcal{M} &= \begin{pmatrix} \hat{m} & 0 & 0 \\ 0 & \hat{m} & 0 \\ 0 & 0 & m_s \end{pmatrix} \\ \Phi &= \{ \pi^+; \pi^0; \pi^-; K^+; K^0; \bar{K}^0; K^- \} \\ \hat{m} &= \frac{1}{2} (\hat{m}_u + \hat{m}_d) = 7 [MeV].\end{aligned} \quad (10)$$

The pion nucleon Σ -term is calculated by introducing the chiral symmetry breaking (χ SB) Hamiltonian $\mathcal{H}_{\chi SB}$ according to the diagrams of figure 9 into the quark and the Goldstone boson (dashed lines) propagator.

The results are contained in table 1. The contribution of the valence quarks is only 13.1 MeV, while the pion cloud contributes the largest part to the pion-nucleon Σ term. The final result is in good agreement with the

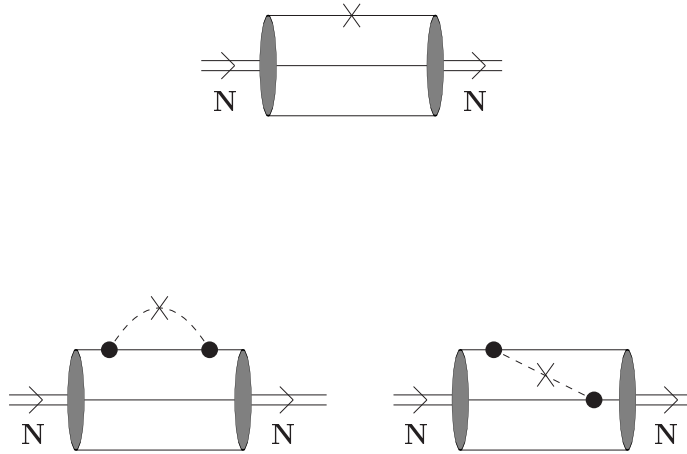


Figure 9. Diagrams for the pion nucleon Σ -term in SU(3) flavour. The cross indicates the introduction of the chiral symmetry breaking term $\mathcal{H}_{\chi SB}$ into the quark (solid lines) and the pseudoscalar Goldstone boson (dashed line: indicating pion, kaon and η meson propagators).

extraction of this quantity by J. Gasser from the data (which is controversial).

Table 1. Contribution of the valence quarks $\sigma(q)$. The pion-nucleon Σ term is the sum of the valence contribution $\sigma(q)$, the pion cloud $\sigma(\pi)$, the kaon cloud $\sigma(K)$ and the η cloud $\sigma(\eta)$. The theoretical error of $\sigma(\text{total})$ is due to the uncertainty in the mean square radius of the quark content of the nucleon $\langle r^2 \rangle = 0.6 \pm 0.1 [fm^2]$.

	<i>MeV</i>
$\sigma(q)$	13.1
$\sigma(\pi)$	30.2
$\sigma(K)$	1.7
$\sigma(\eta)$	0.08
$\sigma(\text{total})$	45 ± 5
$\sigma(\text{exp})$	≈ 45

Different contributions of the valence quarks q , of the pion cloud π , of the kaon cloud K and the eta cloud η to the pion-nucleon Σ term. The sum is compared with the experimental value, extracted by J. Gasser from the

20

data.

2.2. Nuclear Structure and VAMPIR

The standard approach to describe the structure of light nuclei is presently the shell model, while in heavier nuclei one uses mainly the Quasi-Particle Random Phase Approximation (QRPA).

Apart of these approaches one uses in light nuclei up to about mass number 10 the Green's function Monte Carlo method¹⁴. In heavier nuclei one can use the Monte Carlo shell model approach of Otsuka and co-workers¹⁶ and the Tuebingen VAMPIR (Variation After Mean field Projection In Realistic model spaces and with realistic forces)¹⁵. The shell model Monte Carlo method and also the VAMPIR approach select very carefully the configurations which are included in the diagonalization to find the many-body nuclear wave function. In this way the VAMPIR approach can obtain with three to five projected Hartree-Fock-Bogoliubov configurations the same quality as the shell model with several million configurations. The VAMPIR approach starts from the quasi-particle transformation and the intrinsic Hartree-Fock-Bogoliubov wave function.

$$\begin{aligned}
 \alpha_i^+ &= \sum_a \{A_{ai} c_a^+ + B_{ai} c_a\} \\
 |HFB\rangle \equiv |\rangle &= \prod_{all\ i} \alpha_i |0\rangle \\
 E_{JM}^{\pi,Z,N} &= \frac{\langle HFB | \hat{H} \hat{P}_{JM} \hat{P}_\pi \hat{P}_z \hat{P}_N | HFB \rangle}{\langle HFB | \hat{P}_{JM} \hat{P}_\pi \hat{P}_z \hat{P}_N | HFB \rangle} \\
 &= f(A_{ai}, B_{ai}) = Minimum. \tag{11}
 \end{aligned}$$

The first Hartree-Fock-Bogoliubov (HFB) configuration is found by minimizing the energy E_{JM} after projection onto good symmetries like angular momentum, angular momentum projection, parity, time reversal symmetry, proton number and neutron number as a function of the coefficients in the quasi-particle transformation A_{ai} and B_{ai} . As more symmetries one breaks in the quasi-particle transformation from the particle creation and annihilation operators c_a^+ and c_a as better the final wave function will be. But one has to project the HFB wave function on all good symmetries before minimization of the energy. Further configurations are found by requesting orthogonality of the new configurations with the previous ones by Schmidt orthogonalization.

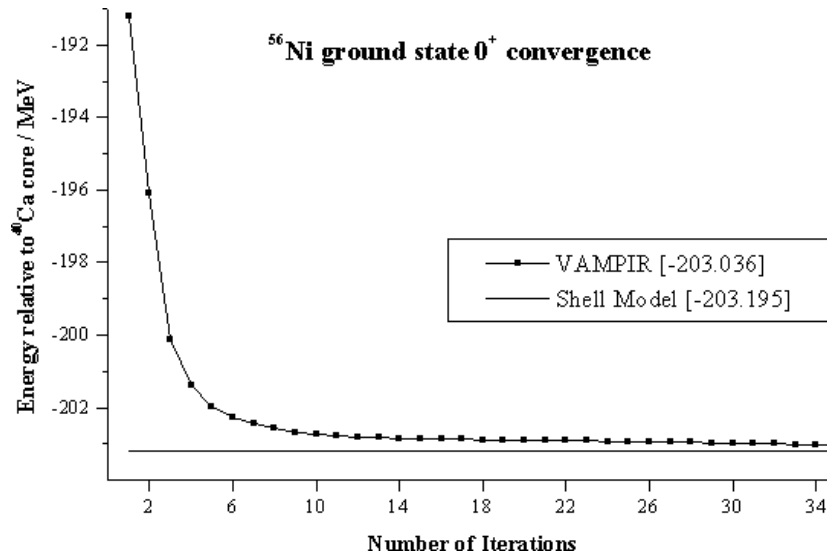


Figure 10. Bound state 0^+ binding energy of ^{56}Ni relative to ^{40}Ca convergence of the VAMPIR approach with a single configuration as in eq. (11) compared with a shell model diagonalization (solid straight line) with more than 15 million configurations of the Strassburg-Madrid group.

Figure 10 shows the convergence of the minimization of the energy of the 0^+ state (11) of ^{56}Ni compared with the shell model calculation of more than 15 million configurations. In the VAMPIR approach one has only one configuration, but the model space is chosen to be the pf-shell as in the shell model approach. In both calculations the same Hamiltonian is used.

An usual restriction in the shell model calculations for the pf-shell nuclei is to allow in the $f_{7/2}$ shell for the protons and the neutrons only six holes (maximum number of holes would be 8). If one uses in the VAMPIR approach two configurations, one obtains a lower energy than the shell model approach with this truncation. With five configurations in a VAMPIR approach we reach a lower energy than the shell model Monte Carlo approach¹⁶ with 30 configurations.

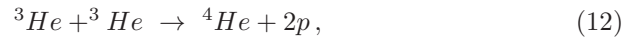
The VAMPIR approach is able to use a larger basis than the pf-shell and in this case one reaches a lower energy than the best shell model calculations with up to 100 million configurations, which must be restricted to the pf-shell.

Thus one sees it pays to select carefully the configurations which one is including into the nuclear structure calculations. The shell model needs

so many configurations, because one takes all possible configurations in a non-optimal single particle and many-body basis.

2.3. Nuclear Astrophysics at the Gamow Peak

Nuclear reactions relevant for the formation of the elements in the stars are far below the Coulomb barrier. A very interesting example is the fusion reaction

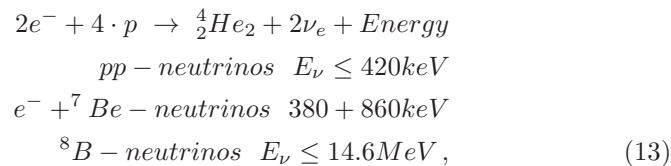


which essentially determines the high energy neutrino flux produced by the sun. Since the reaction is extremely weak at the temperatures of about 15 million degrees in the sun, one measures the reaction cross-section in the laboratory at higher energies and extrapolates with the astrophysical S-factor down to the energy (Gamow peak), where the reaction really happens in the sun.

A collaboration from Napoli and Bochum was now able to measure for the first time in the Gran Sasso this reaction at the Gamow peak (see figure 11).

2.4. The Solar Neutrino Problem

In the sun hydrogen is burning into helium



in a reaction network, which leads to the production of ${}^4\text{He}$. Neutrinos are produced at different places. The main neutrino sources as indicated in eq. (13) is the proton-proton chain, the electron capture in ${}^7\text{Be}$ and the beta decay of ${}^8\text{B}$.

Different detectors investigated the neutrino flux from the sun and found all fewer neutrinos than expected from the standard solar model. The Cl detector in the Homestake mine of Davies measures mainly the B neutrinos and partially also the ${}^7\text{Be}$ neutrinos from the 860 keV line. The detector finds about 34 % of the neutrinos expected. The two Ga detectors GALLEX in the Gran Sasso and the SAGE in the Caucasus have a very low threshold

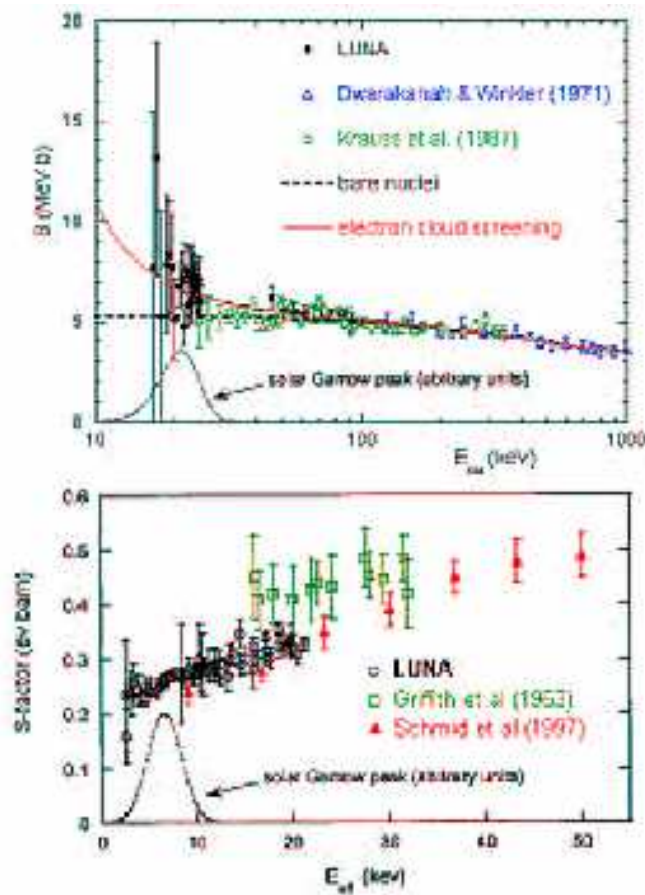


Figure 11. Cross-section of the fusion reaction ${}^3\text{He} + {}^3\text{He}$ of eq. (12) measured by the Luna collaboration in the Gran Sasso over 12 order of magnitudes until down to the Gamow peak.

of about 230 keV and are mainly sensitive of the neutrinos from the proton-proton chain and to the two discrete lines from ${}^7\text{Be}$. These detectors find 59 and 58 % of the neutrinos expected.

The Cherenkov detectors Kamiokande and Super-Kamiokande in Japan, which are only sensitive to the high energy ${}^8\text{B}$ neutrinos measure 55 and 46 % of the neutrinos expected. The breakthrough came from the Cherenkov detector with heavy water D_2O in the Sudbury Neutrino Observatory (SNO). SNO measures at the same time charge and neutral current reac-

tions. It also can separate the neutrino reactions on nucleons from the ones on electrons. By using for the charge current reactions on electrons the precise measurement by Super-Kamiokande one can separately determine the total neutrino and the electron neutrino flux from the sun. This separation is only possible by measuring the charge current reaction on the neutron (see figure 12), which requires heavy water.

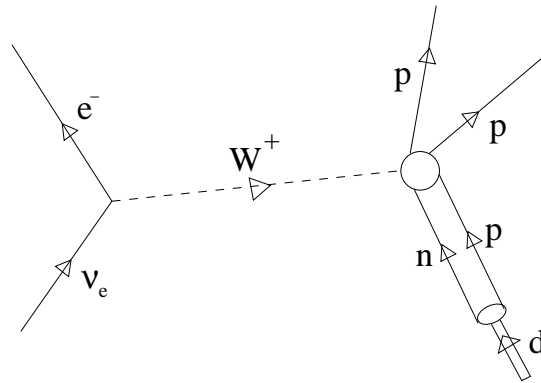


Figure 12. Charge current reaction of an electron neutrino on the deuteron. This charge current reaction cannot be measured at the neutrons in ^{16}O , since they are too strongly bound.

By separating with the angular distribution the charge current reaction on a neutron from the charge and the neutral current reaction on an electron and by using the precise measurement of Super-Kamiokande for the charge current reaction and the neutral current reaction on an electron, one is able to determine separately the electron neutrino flux and the total neutrino flux from the sun. The total neutrino flux from the sun is exactly the one expected from the standard solar model for electron neutrinos. So one concludes that no electron neutrinos from the sun are missing. They only oscillated in muon or tauon neutrinos. The SNO data also exclude within the precision of the measurement (which is not too good) oscillations into sterile neutrinos.

So finally we have no neutrino puzzle. We must only understand the neutrino oscillations more in detail. This means we must get to know the neutrino masses and the neutrino mixing matrix. SNO favours the large mixing angle solution for solar neutrinos and excludes practically the small mixing angle solution. So the mixing of the first and the second mass eigenstates is about $\theta_{12} \cong 35^\circ (\pm 5^\circ)$ and from the atmospheric neutrinos

we find $\theta_{23} = 45^\circ$, while the data seem to suggest $\theta_{13} \cong 0^\circ$ (with a large error). $\theta_{13} = 0$ would not allow CP violation in the neutrino sector. Thus a precise determination of θ_{13} is very important.

3. Conclusion

It is difficult to make predictions, especially if it concerns the future. I tried to extrapolate topics of which I think they are interesting presently and will be interesting also in the next future.

- (1) We shall use more and more lattice QCD and also analytical methods to solve QCD to determine properties of hadrons. On the other side one must show that the present effective field theories can be justified by QCD as a low energy limit like chiral perturbation theory. As a candidate for such an effective field theory which includes pseudoscalar Goldstone bosons and quarks I discussed the perturbative chiral quark model (P χ QM), which we developed in Tuebingen.
- (2) Due to the advent of radioactive beams nuclear structure has a renaissance. As an approach to get better and better solution of the nuclear structure problem also in heavier nuclei, I discussed VAMPIR¹⁵, which with very few configurations can obtain the same quality of results as shell model calculations with several million configurations.
- (3) Ultrarelativistic heavy ion collisions will study (and detect) in the future more in detail the phase transition from nuclear to quark matter.
- (4) With the radioactive beams we will be able to study more and more reactions which are relevant for nuclear astrophysics, especially for the formation of the elements in the stars. Measurements of astrophysical relevant reactions until down to the Gamow peak are now possible by small accelerators in underground laboratories.
- (5) Neutrino physics is at the moment a very fast developing field. It seems that the solar neutrino problem is practically solved. One still has to verify if the data from LSND (Los Alamos Scintillator Neutrino Detector) are correct. For this the experiment Mini-BooNE is starting to take data at Fermi Lab. We wait for more data from SNO (Sudbury Neutrino Observatory) and more data from Long Baseline neutrino oscillation experiments to determine the neutrino mixing matrix.
- (6) Especially interesting are tests of new physics beyond the standard

model of Grand Unified and Supersymmetric theories. Such models can be tested in rare decays. Among them rates very high the neutrinoless double beta decay, which can distinguish between Dirac and Majorana neutrinos, and the measurement of the electric dipole moment of the neutron.

References

1. H. Leutwyler, *Ann. of Physics* (1994).
2. S. Weinberg, *Phys. Rev.* **130**, 776 (1963).
3. S. Weinberg, *Physica* **96 A**, 327 (1979).
4. D. Hadjimichel, G. Krein, S. Szpigel, J. S. Da Veiga, *Ann. of Physics* **268**, 105 (1998).
5. A. Salam, *Nuovo Cimento* **25**, 224 (1962).
6. M. Strohmeier, Th. Gutsche, A. Faessler, R. Vinh Mau, *Phys. Lett.* **B438**, 21 - 26 (1998);
*Phys. Rev.***D 60**; 010 (1999);
*Acta Phys. Polon.***B31** 2657 (2000);
Nucl. Phys. **A684** 345 (2001).
7. C. Amsler, *Phys. Lett.* **B 541**, 22 (2002).
8. A. Faessler, F. Fernandez, **Phys. Lett.** **124 B**, 145 (1983);
K. Bräuer, A. Faessler, F. Fernandez, K. Shimizu, *Z. Phys.* **A 320**, 609 (1985);
A. Valcarse, A. Buchmann, F. Fernandez, Y. Yamauchi, A. Faessler, *Phys. Rev. C* **50**, 2246 (1994);
A. Valcarse, A. Faessler, F. Fernandez, *Phys. Lett.* **B 345**, 367 (1995) and
Phys. Rev. C **51**, 1480 (1995).
9. A. Faessler, V. I. Kukulín, I. t. Obukhovskiy, V. N. Pomerantsev, *J. Phys.***G 27**, 1851 (2001).
10. S. Frauendorf, *Rev. Mod. Phys.***73**, 463 (2001).
11. R. M. Clark et al., **A 562**, 121 (1993) and S. Frauendorf and F. Doenau, *Proceedings of Oak Ridge Conference on High Angular Momentum, 1982*.
12. D. J. Jenkins et al., nucl-ex/0007004.
13. A. Poves, J. Sanches-Solano, E. Caurier, F. Nowacki, *Nucl. Phys.* **A 694**, 157 (2001) and **A 693**, 374 (2001).
14. R. B. Wiringa, S. C. Pieper, J. Carlson, V. R. Pandharipande, *Phys. Rev. C* **62**, 014001 (2000).
15. T. Hjelt, K. W. Schmid, A. Faessler, *Nucl. Phys.* **A 697**, 164 (2002);
A. Petrovici, K. W. Schmid, A. Faessler, *Nucl. Phys.* **A 689**, 707 (2001).
16. M. Honma, T. Otsuka, B. A. Brown, T. Mizusaki, *Phys. Rev. C* **65**, 061301 (2002).
17. T. Niksik, D. Vretenar, P. Pirelli, P. Ring, *Phys. Rev. C* **66**, 024306 (2002).
18. R. Bernabei, *Prog. Part. Nucl. Phys.* **48**, 263. (2002).
19. M. Milgrom, *Scientific American*, August 2002.
20. H. V. Klapdor-Kleingrothaus, A. Dietz, I. V. Krivosheina, **Part. Nucl. Lett.** **110**, 57 (2002).

21. V. E. Lyubovitskij, T. Gutsche, A. Faessler, R. Vinh Mau, *Phys. Lett.* **B520**, 204 (2001) and *Phys. Rev.* **63**, 054026 (2001).
22. V. E. Lyubovitskij et al., *Phys. Rev.* **C65**, 025202 (2002).
23. V. E. Lyubovitskij, P. Wang, T. Gutsche, A. Faessler, hep-ph/0207225 and hep-ph/0205251.
24. R. K. Bhaduri, *Models of the Nucleon*; Addison Wesley Publishing Company, Redwood City, 1988.
25. A. Thomas, W. Weise, *The Structure of the Nucleon*; Wiley-VCH, Berlin, 2000.
26. V. E. Lyubovitskij, Th. Gutsche, A. Faessler, R. Vinh Mau, *Phys. Lett.* **B 520**, 204 (2001) and V. E. Lyubovitskij et al., *Phys. Rev.* **C65**, 025202 (2002).
27. M. A. Ivanov, V. E. Lyubovitskij, *Phys. Rev.* **D 56**, 348 (1997).
28. M. A. Ivanov, M. P. Locher, V. E. Lyubovitskij, *Few Body Systems* **21**, 131 (1996).
29. A. Poves, J. Sanchez-Solano, E. Caurier, F. Nowacki, nucl-th/0210069.
30. SNO-Collaboration, *Phys. Rev. Lett.* **89**, 011302 (2002) and *Phys. Rev. Lett.* **89**, 11301 (2002).